Biomaterials Science

The bifunctional regulation of interconnected Zn-incorporated ZrO2 nanoarrays in antibiosis and osteogenesis

Journal:	*Biomaterials Science*
Manuscript ID:	BM-ART-07-2014-000263.R1
Article Type:	Paper
Date Submitted by the Author:	29-Aug-2014

Complete List of Authors:	Zhu, Zhi Hong; Institute of Nano-science and Nano-technology, College of Physical Sience and Technology,Central China Normal University Cheng, Haoyan; Institute of Nano-science and Nano-technology, College of Physical Sience and Technology,Central China Normal University Mao, Lin; Hubei Key Laboratory of Genetic Regulation and Integrative Biology, School of Life Sciences, Central China Normal University Xu, Xing; School of Life Sciences, Central China Normal University Zeng, Yan; College of Chemistry and Technology, Central China Normal University Lan, Danni; Institute of Nano-science and Nano-technology, College of Physical Sience and Technology, Central China Normal University Hu, Hao; Institute of Nano-science and Nano-technology, College of Physical Sience and Technology, Central China Normal University Wu, Xu; Institute of Nano-science and Nano-technology, College of Physical Sience and Technology,Central China Normal University You, Huihui; Hubei Key Laboratory of Genetic Regulation and Integrative Biology, School of Life Sciences, Central China Normal University Yang, Xu; Hubei Key Laboratory of Genetic Regulation and Integrative Biology, School of Life Sciences, Central China Normal University Li, Rui; Hubei Key Laboratory of Genetic Regulation and Integrative Biology, School of Life Sciences, Central China Normal University

Cite this: DOI: 10.1039/c0xx00000x

www.rsc.org/xxxxxx

ARTICLE TYPE

The bifunctional regulation of interconnected Zn-incorporated ZrO_2 nanoarrays in antibiosis and osteogenesis

Haoyan Cheng,‡[a] Lin Mao,‡[b] Xing Xu,[c] Yan Zeng,[d] Danni Lan,[a] Hao Hu,[a] Xu Wu,[a] Huihui You,[b] Xu Yang,[b] Rui Li*[b] and Zhihong Zhu*[a]

Received (in XXX, XXX) Xth XXXXXXXXX 20XX, Accepted Xth XXXXXXXXX 20XX
DOI: 10.1039/b000000x

New generational biomaterials should be designed to bear long-term antibacterial activity, biocompatibility and even osteogenesis facilitation. In this study, the bifunctional regulation of antibiosis and osteogenesis is realized by the highly-ordered and interconnecting Zn-incorporated ZrO_2 nanoarrays, which are prepared by hydrothermal approach with the precursor hydrolyzed *in situ* and allow long-term controllable Zn release. The content of incorporated Zn can be easily controlled by pH of HCl solution used for etching. All Zn-incorporated nanoarrays show good antibacterial properties against both *Escherichia coli* (*E. coli*, gram-negative) and *Staphylococcus aureus* (*S. aureus*, gram-positive), as indicated by high antibacterial rates and apparent inhibition zone. Analysis of the biocompatibility confirms that the hybrid nanoarrays could cause varying degrees of promotion for the adhesion and spreading of MC3T3-E1 cells. Zn incorporated ZrO_2 nanotubes balance antibiosis and osteogenesis delicately, as proved by the up-regulated MTT and ALP activity, as well as the increasing of bone-related gene expression (mRNA level of OCN, OPN and BMP-2). The novel bone implant materials with better antibacterial property can promote the osteogenesis, which have promising applications in biomedical devices and antibacterial control systems.

1. Introduction

Implant materials which possess both long-term antibacterial ability and excellent biocompatibility need to be tailored due to the fact that the implant-associated infections remain one of the most serious clinical complications.[1] Generally, *E. coli* and *S. aureus* are typically susceptible bacteria because of their biofilm mode in growth during and after implant surgery.[2] The biofilm makes the bacteria highly resistant to the host defense and antibacterial agents, thereby leading to persistent and chronic infections.[3] Accordingly, improving the antibacterial characteristics on the surface of implants and reducing the probable infections would increase the success rate of bone transplantation surgery.

A bundle of studies have been done mainly focused on factors affecting surface bacteria adhesion by modifying surface with organic antibacterial agents such as hydrogels, chitosan and gentamicin.[4-6] However, the fabrication process is usually complex and costly. Specifically, the adhesion between the Ti surface and organic agents with bioactivity is unstable particularly at high temperature or pressure. By contrast, inorganic antibacterial materials such as metal oxides are robust and durable. Therefore they have key advantages of stability and longer shelf life.[7] ZnO has captured increased interest for its application in biomedical therapy over the past decade. Nanoscaled ZnO in aqueous solution can generate active oxygen radicals (ROS) such as hydroxyl radical, hydrogen peroxide and superoxide,[8, 9] which will result in oxidative damage of bacterial cells, making it outstanding for the application as bactericide in daily life. The antimicrobial activity of ZnO nanoparticles has been studied with different pathogenic and nonpathogenic bacteria such as *S. aureus* and *E. coli*.[10, 11] The released zinc ions are also commonly added as an antimicrobial agent to many oral healthcare products for its multiple inhibitory actions in bacterial, such as glycolysis, transmembrane proton translocation and acid tolerance.[12] It was documented that Zn-incorporated coatings showed excellent vitro antibacterial activity against *S. aureus* and *E. coli*, and the ability to inhibit bacteria could be improved by increasing Zn content in the coatings.[1] In addition, previous studies have demonstrated that Zn showed strongly anti-inflammatory potential by decreasing levels of the pro-inflammatory mediator inter-leukin-8 and the matrix metallo-proteinase-9.[13]

Besides its outstanding antibacterial performance, as an essential trace element, Zn is reported to be involved in bone metabolism and it plays key roles in osteoblasts activity as evidenced by the increased cell adhesion and proliferation.[14, 15] Furthermore, Zn exerts direct effect on bone mineralization because of its effect on nucleation and mineral growth, which is of great significance for skeletal development.[16] Numerous studies *in vivo* had documented that the Zn-modified implant exhibited excellent osseointegration between bone and implant,[17] while the extracellular matrix calcification in osteoblasts was inhibited

in the absence of Zn, which resulted in the decrease of matrix proteins, type I collagen and ALP activity.[18] Likewise, nucleic acid metabolism, cell growth, division and tissue repair also require sufficient supply of Zn.[14]

Evidences of the beneficial effects brought by Zn in antibiosis and osteogenesis have motivated us to incorporate Zn into titanium-based implants for skeletal tissue applications. Notwithstanding, fast release of Zn is adverse to long-term antibacterial activity and overdosage of Zn is a potential hazardous factor for osteoblasts. The balance between antibacterial property and osteogenesis is important for surgical implantation. Therefore, it is of vital importance to develop suitable nanoreservoirs with efficient Zn release system for long-term antibacterial activity, bio-safety and osteogenesis. Depositing antibacterials into TiO_2 nanotubes is known to be the most common method.[19-21] However, it is still a challenge to uniformly deposit appropriate amount of antibacterial drugs into TiO_2 nanotubes because deposition at the pore entrance is easier than that in the internal part of the nanotubes due to the existence of surface tension. Therefore, it is difficult to control the release of antibacterial drugs and eliminate cytotoxicity caused by high concentration antibacterial drugs.[22] In order to realize the controlled release of Zn, in our experiment, highly ordered ZnO nanorods with compatible density and dimensionality were prepared on titanium substrate first, and then zirconia (ZrO_2) was further coated onto the ZnO nanorods by *in situ* hydrolyzed precursor. Similar to TiO_2, ZrO_2 nanotubes are also promising implant materials for orthopedic applications such as artificial knees and dental implants owing to their strong corrosion resistance and long-term stability,[23] as well as *in vivo* biocompatibility.[24, 25] It was found that the adhesion and spreading of mesenchymal stem cells were enhanced on ZrO_2 nanotubes with diameter of ~15-30 nm.[26] The structure of ZrO_2 nanoarrays was controlled by the regulation of sacrificial template and Zn content was controlled by the dissolution condition in our experiments. The antibacterial activity of ZrO_2 nanoarrays with different Zn contents was elucidated along with cell-material interactions.

2. Materials and methods

2.1 Sample fabrication

Firstly, Ti foils with the dimension of 3 cm × 3 cm were ultrasonically cleaned in acetone, ethanol and deionized water sequentially. Then, the hybrid nanorods were synthesized by three steps as shown in Fig. 1: (1) hydrothermal synthesis of ZnO nanorods (ZnO-NR) on Ti foils, (2) coating of ZrO_2 shell on the ZnO nanorods by precursor hydrolyzing *in situ* and (3) dissolution of ZnO. Firstly, ZnO nanorods (ZnO-NR) were prepared as previous work via seed-assisted hydrothermal method.[27] Briefly, zinc acetate (0.025 mol) and diethanol amine (0.06 mol) were dissolved in ethanol (100 mL) solution at 60 °C in constant intense stirring for 1 h to yield clear and homogeneous sol. Then, the sol was spin-coated onto the treated Ti foils and annealed at 500 °C for 1 h to produce ZnO seed layer. The seeded substrates were hydrothermal treated in precursor solution (50 mL) containing zinc nitrate (10 mM), ammonium fluoride (20 mM) and ammonium hydroxide (2.5 mL) at 70 °C for 8 h to produce ZnO-NR. Next, as for the synthesis of ZrO_2 coating layer, ZnO-NR grown on Ti was dipped into mixed solution (4 mL) with ethanol and zirconium(Ⅳ) propoxide (V: V = 10: 1) for 1 h and then the immersed products were annealed at 500 °C for 1 h, resulting in the core-shell structure nanorods (CS-NR). Finally, samples with top away structure and nanotube structure denoted as TA-NR and ZrO_2-NT containing different contents of Zn can be obtained by etching CS-NR in 100 mL diluted HCl acid (pH = 3 and pH = 2.5) for 24 h .

2.2 Surface characterization

The obtained products were characterized with X-ray diffraction (XRD, X'Pert PRO MRD, PANalytical, Netherlands), field-emission scanning electron microscopy (SEM; JEOL, JSM-6700F, Japan), and transmission electron microscopy (TEM; JEM-2100 (HR), 200 kV). The EDS test was carried on the energy dispersive X-ray spectrometer (EDS) which was equipped on the SEM of QUANT200.The aqueous wettability of different substrates was analyzed by contact angle measurements using a Model 200 video-based optical system. The images of water drops on the sample surface were recorded by a digital CCD camera, and then analyzed with software supplied by the manufacturer.

2.3 Zn ion release

To detect the release time profile of Zn ion *in vitro*, each sample with the dimension of 1 cm × 1 cm was immersed in 5 mL PBS for 1 day and then removed and immersed in another 5 mL fresh PBS. This process was repeated for 21 days to generate solutions at different time points. The amounts of Zn released from different samples were analyzed by inductively-coupled plasma atomic emission spectrometry (ICP-AES, IRIS Advantage ER/S).

2.4 Antibacterial assay

E. coli and *S. aureus* were both selected to evaluate the antibacterial activity of different samples. *E. coli* was cultured in Luria-Bertani (LB) medium, and *S. aureus* was cultured in beef extract-peptone (BEP) medium at 37 ℃ for one day. The bacterial suspension was diluted to an initial concentration of approximately 1×10^6 CFU/ mL. All samples were sterilized by autoclaving at 121 ℃ for 30 min before experiment. Each specimen was exposed to 200 μL bacteria suspension at 37 °C for one day. At the end of the incubation period, the culture medium was collected to determine the viable counts of planktonic bacteria through dilution method of plate counting. The antibacterial rate for planktonic bacteria was calculated based on the following formulas:

$$C = \frac{A-B}{A} \times 100\%$$

Where A indicates the colony forming units (CFUs) of control group with no specimen, and B is the CFUs of experimental group. Bacteria adhered on each specimen were fixed with 3% glutaraldehyde at 4 °C for 1 h, then dehydrated in graded ethanol series, and examined by scanning electron microscopy. As for bacteriostatic ring assay, *E. coli* and *S. aureus* were adjusted to a concentration of 1×10^7 CFU/ mL. 100 μL bacterial suspensions were spread onto agar plates and then the samples were lightly placed on the inoculated agar plates and incubated at 37 °C for 24

h, 48 h and 72 h, respectively. A series of representative pictures were taken with an optical camera (Panasonic, DMC-FZ50).

2.5 Cell culture

Newborn mouse calvaria-derived MC3T3-E1 cells were obtained from a preservation center for typical culture in Wuhan university (Wuhan, China). Cells were cultured in a-MEM (HyClone) containing 10% (v/v) fetal bovine serum (FBS; Gibco) and 1% penicillin/streptomycin and incubated in a humidified atmosphere of 5% CO_2 at 37 °C. Cell culture medium was changed every three days. The cells of passage 2-4 were used in the experiments.

2.6 Cell morphology observation

Cell morphology was observed by SEM (JSM-6700F) and CLSM (Leica, Germany) to evaluate the attachment behaviors of MC3T3-E1 cells on different materials. MC3T3-E1 cells were seeded in 96-well plates at an initial density of 1×10^4 cells/ well. After 6 h culturing, cells were rinsed with phosphate-buffered saline, fixed with 3% glutaraldehyde, dehydrated in a graded ethanol series, freeze-dried, sputter coated with gold, and observed by SEM. For the immunofluorescence microscopy observation, after incubation for 24 h on different samples at an initial density of 1×10^4 cells/ well, the attached cells were fixed in 4% paraformaldehyde for 30 min at 4 °C. And then, 0.1% Triton X-100 was added on the samples for 5 min before staining the actin cytoskeletons. Samples were incubated with FITC-Phalloidin (Sigma) at room temperature in the dark for 60 min. Finally, the nuclei were stained with 40, 6-diamidino-2-phenylindole dihydrochloride (DAPI, Sigma). The stained samples were finally mounted with 90% glycerinum for CLSM observation and the cell number on each sample was also counted.

2.7 Cell viability detection

MTT assay was used to evaluate the viability of MC3T3-E1 cells. MC3T3-E1 cells were plated on each sample in 96-well plates at an initial seeding density of 1×10^4 cells/ well. After 24 h, 48 h and 72 h of culture, cells were rinsed by PBS. Subsequently, fresh cell culture media was added to the targeted wells, and the MTT dye agent was added in an amount equal to 10% of the culture media volume, according to manufacturer's instructions (MTT kit, Sigma, USA). Then plates were incubated at 37 °C for another 4 h to form formazan, which was later dissolved with addition of dimethyl sulfoxide after removing the MTT containing medium. The absorbance of the final solution was measured using a microplate reader (DNM-9602) at wavelength of 492 nm.

2.8 Lactate dehydrogenase activity assay

Lactate dehydrogenase (LDH) released by cells into the culture media was measured to investigate the cytotoxicity. MC3T3-E1 cells were seeded onto different samples at a density of 1×10^4 cells/ well. After incubation for 24 h, 48 h and 72 h respectively, the culture media was collected and centrifuged, and the activity of LDH in the supernatant was determined following the manufacturer's instructions.

2.9 Alkaline phosphatase (ALP) assay

Alkaline phosphatase (ALP) activity was determined to assess the bone forming ability of MC3T3-E1 cells on the experimental substrate surfaces. After being cultured for 7 and 14 days, respectively, MC3T3-E1 cells on different substrates were lysed by 1% Triton X-100 overnight and then broken by sonic oscillator for 30 min. The cells lysates were centrifuged at 13,500 rpm for 4 min.The ALP activity in the supernatant was determined with ALP assay kit by measuring the absorbance at 405 nm. Bicinchoninic acid (BCA) Protein Assay kit was used to calculate the total protein content, the absorbance was measured at a wavelength of 560 nm using a microplate reader (DNM-9602). Finally, the ALP activity was normalized by total intracellular protein production.

2.10 Quantitative reverse transcription polymerase chain reaction (qRT-PCR)

The expression levels of osteogenesis related genes were determined using the qRT-PCR. Cells were seeded onto different samples at a density of 2×10^5 cells/ well in the 6-well plates, then cultured for 2 weeks and harvested using TRIzol (Invitrogen) to extract the RNA. The obtained RNA was reverse transcribed into complementary DNA using PrimeScript RT reagent Kit (Takara). SYBR green chemistry was used to perform quantitative determinations of the mRNAs for type I collagen (Col-I), osteocalcin (OCN), osteopontin (OPN), bone morphogenetic protein-2 (BMP-2) and a housekeeping gene M-actin following the optimized protocol. The double stranded DNA-specific dye SYBR Green I was incorporated into the PCR buffer provided in the SYBR Premix Ex Taq™ reagent. The temperature profile of the reaction was 95 °C for 10 min, 40 cycles of denaturation at 95 °C for 10 s, annealing at 60 °C (Col-I, OCN, OPN and BMP-2) for 20 s, and extension at 72 °C for 20 s. The M-actin gene was used to correct for differences in RNA isolation, RNA degradation, and the efficiencies of the reverse transcription.

2.11 Statistical analysis

The results were representative of at least three independent experiments and all data were expressed as mean ± standard deviation for n = 5. The statistical analysis was performed with statistical software Origin7.5. $p < 0.05$ was considered to be significant and $p < 0.01$ was regarded to be highly significant.

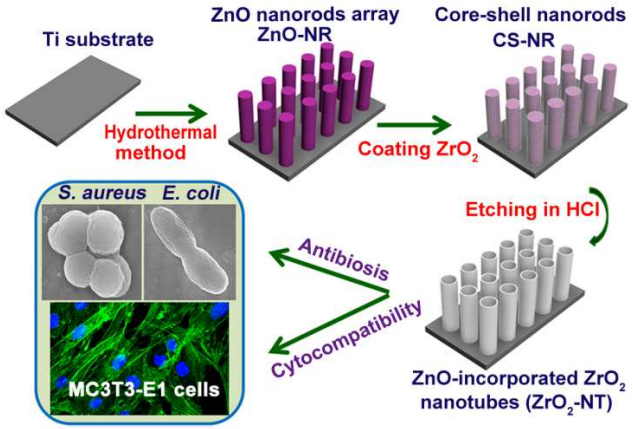

Fig. 1 Schematic illustration of the fabrication of Zn-incorporated nanoarrys and biological assessment.

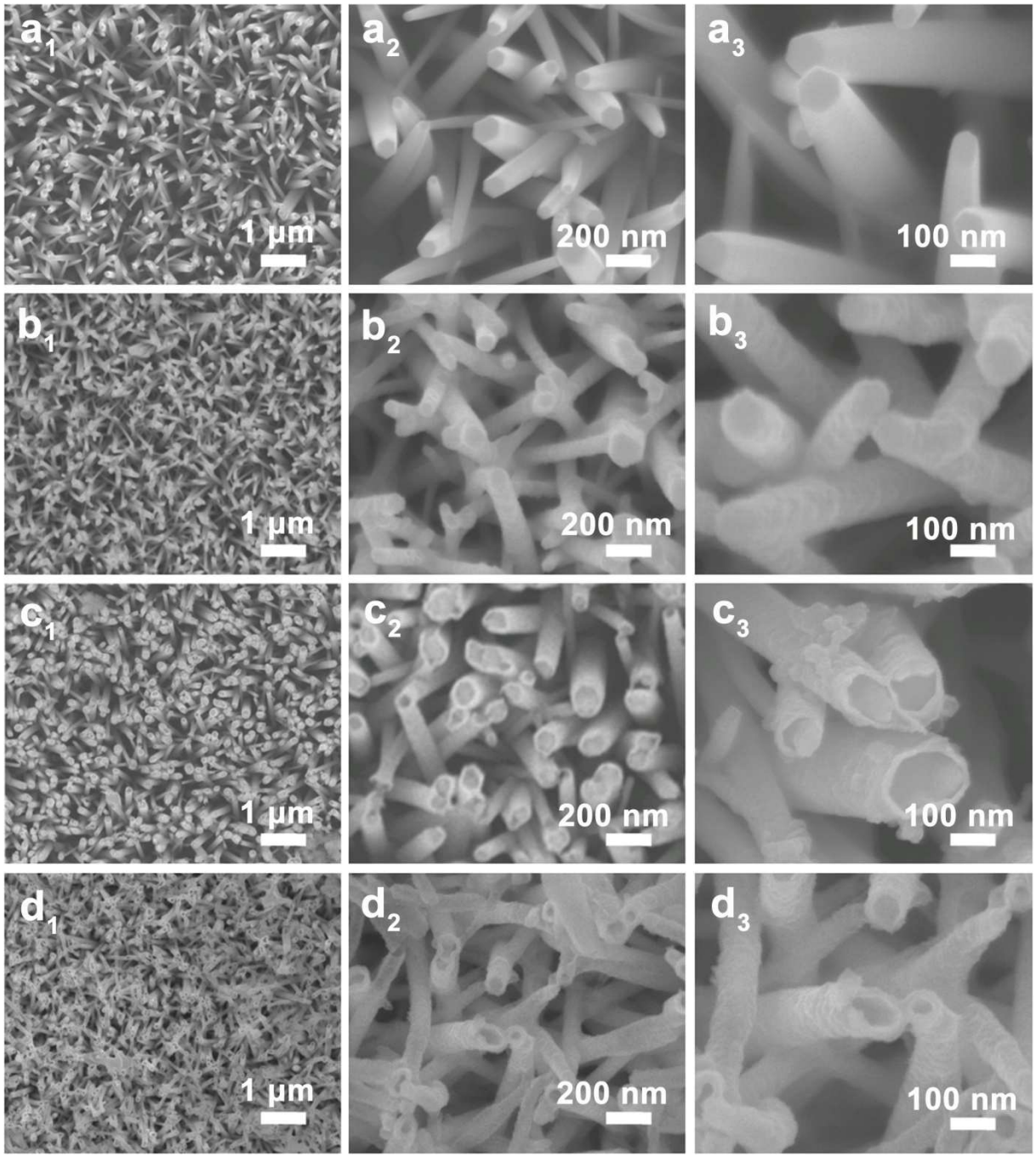

Fig. 2 The SEM of the samples for low and high magnification. ZnO-NR (a_1, a_2, a_3), CS-NR (b_1, b_2, b_3), TA-NR (c_1, c_2, c_3), ZrO_2-NT (d_1, d_2, d_3).

3. Results

3.1 Surface characterization

The Zn-incorporated nanoarrays were synthesized in three steps as shown in Fig. 1. The SEM images of ZnO nanorods (ZnO-NR), core-shell stucture nanorods (CS-NR), top-away structure nanorods (TA-NR) and Zn-incorporated ZrO_2 nanotubes (ZrO_2-NT) are demonstrated in Fig. 2, respectively. It was revealed that highly ordered ZnO nanorods (ZnO-NR) grew on Ti substrates uniformly with the length of 4 μm and diameter of 60 ~120 nm (Fig. 2a). The sufficient space between ZnO nanorods was crucial for the formation of ZrO_2 shell. Fig. 2b revealed that the integration of ZrO_2 into the ZnO array made the nanorods surface coarser without damaging the ordered structure. ZrO_2 shell can be distinguished from ZnO core (Fig. 2c) after CS-NR being etched by diluted HCl solution (pH = 3.0) for 24 h. Zn-incorporated ZrO_2 nanotubes (Fig. 2d) were fabricated after 24 h in diluted HCl (pH = 2.5).

The samples were further investigated by TEM. As shown in Fig. 3a, each ZnO nanorod was shelled by ZrO_2 layer with a thickness of approximate 15 nm. Both the top away structure and nanotube structure of the as-prepared products can be more clearly viewed from Fig. 3b and 3c, in which the outer diameter was shown to be almost the same as the diameter of ZnO nanorods template used,

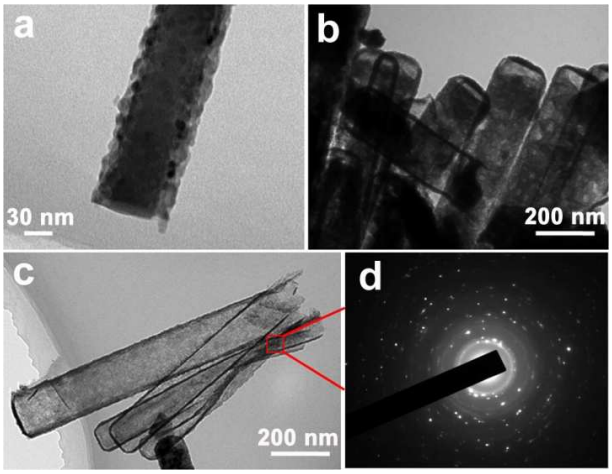

Fig. 3 The TEM analysis on (a) CS-NR, (b) TA-NR, (c) ZrO_2-NT (d) the selected area electron diffraction (SAED) pattern of ZrO_2 -NT.

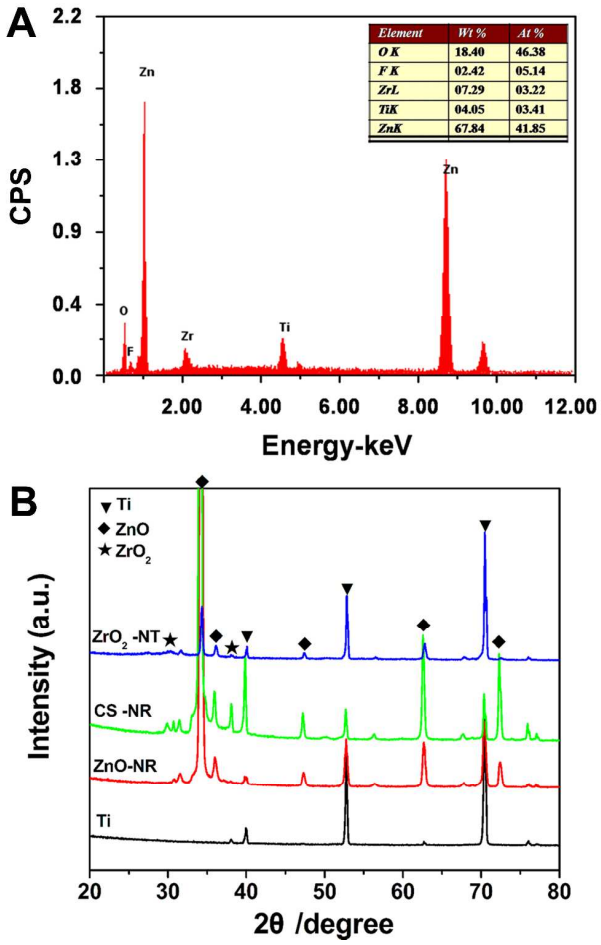

Fig. 4 (A) EDS of the prepared CS-NR. (B) XRD pattern

further illustrating the structure inheritance during the process. The selected-area electron diffraction (SAED) pattern in Fig. 3d showed polycrystalline structure of the ZrO_2 nanotubes.

The chemical compositions of CS-NR were characterized by energy dispersive X-ray spectroscopy (EDS) (Fig. 4A). About 18.4% of O, 2.42% of F, 7.29% of Zr, 4.05% of Ti and 67.84% (mass percent) of Zn were found in CS-NR substrate. Strong signal of Zr element with atomic percentage of 3.22% confirmed that ZnO was successfully coated by ZrO_2. The presence of fluorine in EDS result was derived from the precursor solution containing fluoride salt when fabricating ZnO nanorods. It has been reported that fluoride was widely used as a highly effective anticaries agent in dental implant fields, and fluorine ions can affect bacterial metabolism as an enzyme inhibitor.[28] What's more, a small amount of fluorine had a stronger stimulating effect on cell proliferation and differentiation.[29]

In the XRD spectra (Fig. 4B), as for ZnO-NR, the peak at 2θ = 33° (002) was dominant, with an intensity much higher than that of other peaks, revealing the high c-axis growth orientation of the product. The XRD pattern in Fig. 4B unambiguously disclosed the peak of ZnO in CS-NR, TA-NR and ZrO_2-NT samples, which had great significance for antibacterial activity. However, for ZrO_2-NT, this peak drops sharply due to the decrease of ZnO amount.

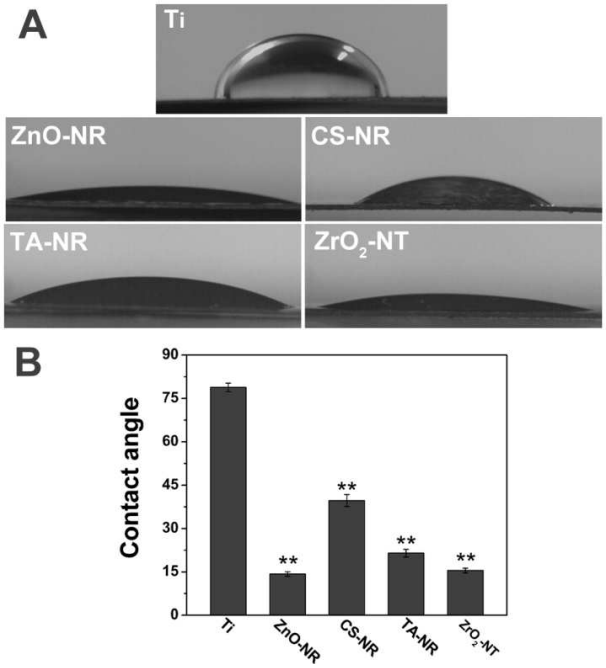

Fig. 5 Water contact angles on different samples. (A) the optical pictures (B) statistical diagram. Error bars represent mean ± SD for n = 5, **p < 0.01 compared to the Ti.

Surface hydrophilicity affects biological functions such as cell adhesion and spreading.[21] As shown in Fig. 5, the water contact angle of ZnO-NR significantly decreased from 78° to 14° compared with that of Ti plate, and the contact angle of CS-NR, TA-NR and ZrO_2-NT were less than 40°. The nanoarrays showed a significantly smaller water contact angle than pristine Ti discs, indicating much higher hydrophilicity. Changes in the water contact angles stem from the surface morphology and chemistry, which was confirmed by Yu et al.[30]

3.2 Zn ion release

The non-accumulated Zn ion released from the CS-NR, TA-NR, ZrO_2-NT was measured by ICP-AES (Fig. 6). It was noteworthy that stable Zn ion release profiles were observed from all three substrates in a time span up to 21 days, which were crucial for long-term antibacterial activity. Thereinto, smaller amount of Zn ion released from ZrO_2-NT than that from CS-NR and TA-NR. This, to a great extent, could be attributed to the smallest quantity

of ZnO in ZrO_2-NT among the three samples.

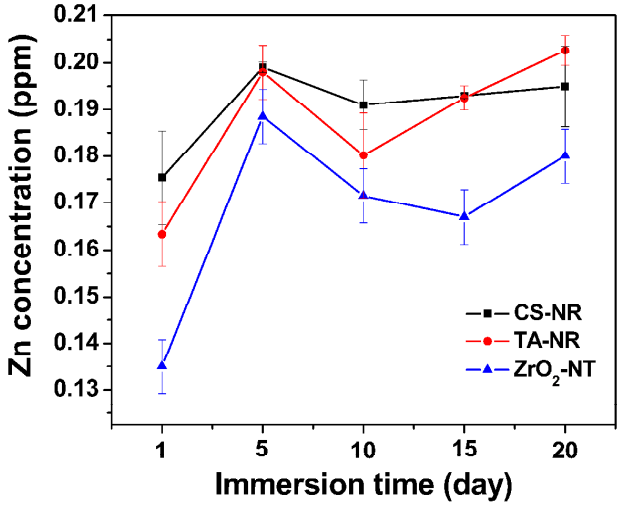

Fig. 6 Non-cumulative Zn ion release from CS-NR, TA-NR and ZrO_2 -NT

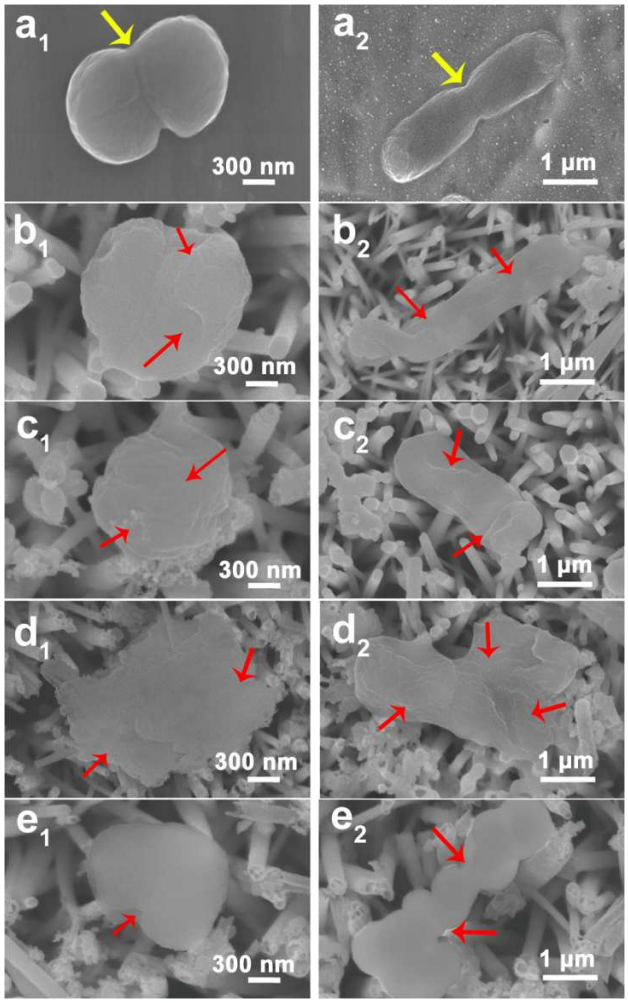

Fig. 7 SEM views of *S. aureus* (a_1-e_1) and *E. coli* (a_2-e_2) seeded on Ti (a_1-a_3), ZnO-NR (b_1-b_3), CS-NR (c_1-c_3), TA-NR (d_1-d_3), ZrO_2-NT (e_1-e_3).

3.3 The antibacterial effect *in vitro*

The morphology of *S. aureus* and *E. coli* on different substrates was observed by SEM after the samples being exposed to 200 μL bacteria suspension at 37 °C for 24 h. Both *S. aureus* and *E. coli* cultured on flat Ti displayed integrated surface and exhibited healthy binary fission (yellow arrows in Fig. 7a_1 and a_2) without notable rupture or released intracellular component on the cell surface. In contrast, *S. aureus* and *E. coli* cultured on ZnO-NR, CS-NR, TA-NR and ZrO_2-NT emerged a wide range of abnormalities with various degrees of twist and deformation (red arrows in Fig. 7), indicating that all nanoarrays with Zn content exhibited a great ability to inhibit bacteria.

In order to assess the antibacterial activity of the samples, at the end of the incubation period of 24 h, the culture medium was collected and re-cultivated on agar plates according to the method of plate counting. Fig. 8A illustrated the representative photographs of bacteria colony number in control group, Ti, ZnO-NR, CS-NR, TA-NR and ZrO_2-NT, respectively. Total plate counts of the largest number were detected on the Ti for both *S. aureus* and *E. coli*, whereas the colony forming units were significantly reduced on other experimental groups. It was noteworthy that neither *E. coli* colony nor *S. aureus* colony could be found on the agar plate of ZnO-NR, suggesting that ZnO had strong antibacterial effect on both two bacteria. Besides, the antibacterial rates of ZnO-NR against *S. aureus* and *E. coli* were approximately 100%. In comparison, the antibacterial rates measured on CS-NR, TA-NR and ZrO_2-NT were all higher than 95% (Fig. 8B and C), illustrating their good antibacterial effect. It can also be inferred that the antibacterial capability was improved with the increase of Zn content. On the contrary, the percentage reduction of *S. aureus* and *E. coli* seeded on Ti reached 18% and 38% below zero, supporting the fact that Ti could significantly multiply the bacteria.

To further investigate the long-term antibacterial property of all substrates, the inhibition zone of ZnO-NR, CS-NR, TA-NR and ZrO_2-NT against both *S. aureus* and *E. coli* were detected after 24 h, 48 h and 72 h of culture, respectively. As shown in Fig. 9A and B, there was no inhibition zone around the pure Ti at anytime for both bacteria, while ZnO-NR exhibited superior antibacterial performance with the largest inhibition zone among those of all samples under the same condition. In general, diameters of the inhibition zone for both bacteria increased gradually with the culture time elongating (Fig. 9C and D), accounting for sustained antibacterial activities of all nanoarrays.

3.4 Cell morphology

To evaluate cell adhesion and growth on different samples, the morphology of MC3T3-E1 cells were monitored by SEM after 6 h of culture (Fig. 10). Clearly, MC3T3-E1 cells cultured on ZnO-NR appeared to be round (Fig. 10b) without any lamellipodia or thin filopodia, illustrating there was no spread on the ZnO nanorods. The lack of lamellipodia is probably due to an inability of cells to establish strong initial adhesion to the substrate, thereby altering the dynamics of cell spreading, which causes cell death.[31] Besides, overdosage of Zn ion would also lead to cytotoxicity.[32] By contrast, most of MC3T3-E1 cells were observed to have much more pronounced protrusion of filopodia with significantly longer configuration and higher degree of contact on pure Ti, CS-NR and TA-NR, especially on ZrO_2 -NT. Immunofluorescent images of cytoskeletal actin (green) with corresponding DAPI nuclear staining (blue) for cells cultured on

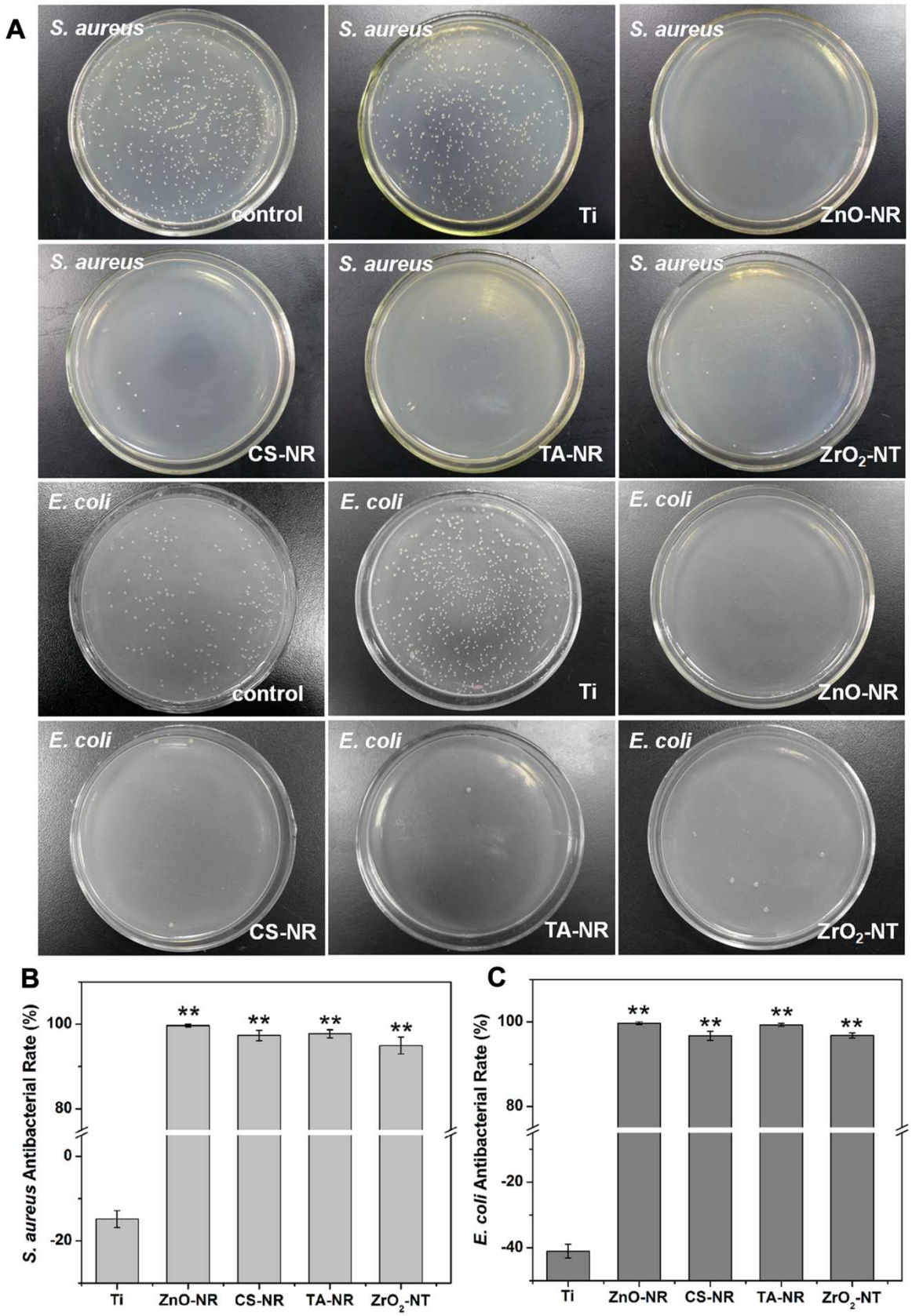

Fig. 8 (A) Typical photographs of recultivated *S. aureus* and *E. coli* colonies on agar plates. The antibacterial rates of (B) *S. aureus* and (C) *E. coli*, **P < 0.01 compared to Ti. All data are expressed as means ± SD and n = 5

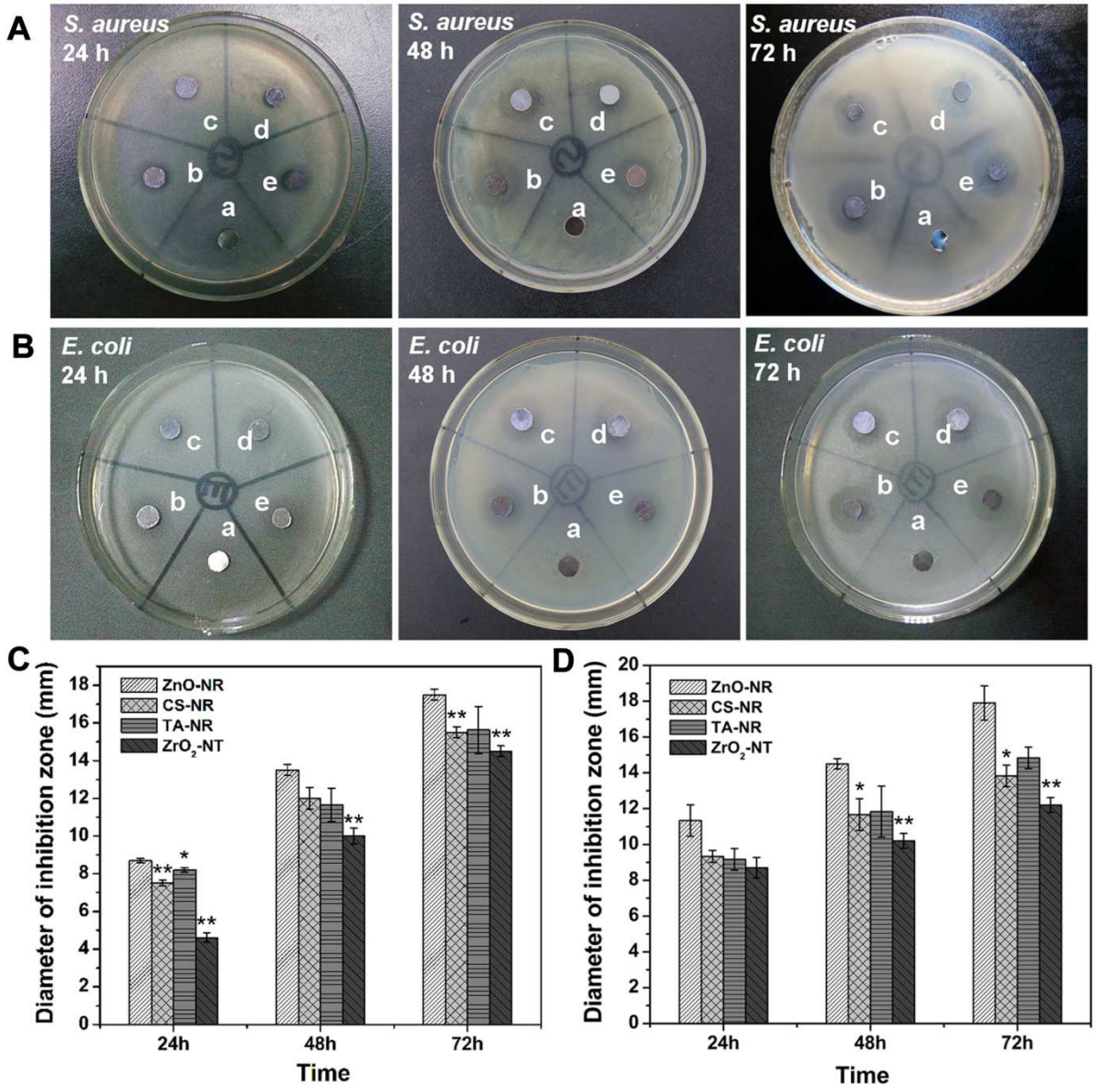

Fig. 9 Images showing the inhibition zone of (A) *S. aureus* cultured on beef extract-peptone medium (B) *E. coli* cultured in Luria-Bertani medium after 24 h, 48 h, 72 h at 37 °C, (a) Ti, (b) ZnO-NR, (c) CS-NR, (d) TA-NR, (e) ZrO_2-NT; diameter of inhibition zone for (C) *S. aureus* and (D) *E. coli*. Error bars represent mean ± SD for n = 5, *p < 0.05, **p < 0.01 compared to Ti.

different substrates were displayed in Fig. 11. Both the morphology and number (Fig. 12A) of adhered cells revealed significantly different surface properties between flat Ti and other nanoarrays. Fluorescence images demonstrated a similar trend of cell spreading on ZnO-NR compared with SEM results. MC3T3-E1 cells on CS-NR and flat Ti were relatively poor in spreading into a spindle shape, behaving as if they were undifferentiated quiescent cells. On the other hand, those cells on TA-NR and ZrO_2-NT showed clear topological configuration with more abundant and well-established filopodia extensions after an identical 24-hour culture, exhibiting a typical polygonal osteoblastic shape. The diversity of cell morphology results from different Zn content of the substrates. Besides, compared with Ti substrate, the nanotopography of the nanoarrays with larger surface areas facilitates cell growth in many different ways, including cell adhesion, cell morphology and proliferation. Previous research indicated that among cell responses to different nanopatterns, ZrO_2 nanotube arrays could provide better environment for cell adhesion and growth,[25] that is why ZrO_2-NT is better than other substrates.

3.5 Cell viability

MTT assay was performed to estimate the proliferation and activity of viable cells on the experimental samples. Fig. 12B showed the optical density (OD) of reaction products of MTT working solution with MC3T3-E1 cells cultured on different substrates after 24 h, 48 h, and 72 h, respectively. Overall, the cell viability increased with the elongation of culture time. MC3T3-E1 cells cultured onto the ZnO-NR substrate displayed the lowest cell viability when compared with others, indicating again the adverse influence of ZnO arrays on the

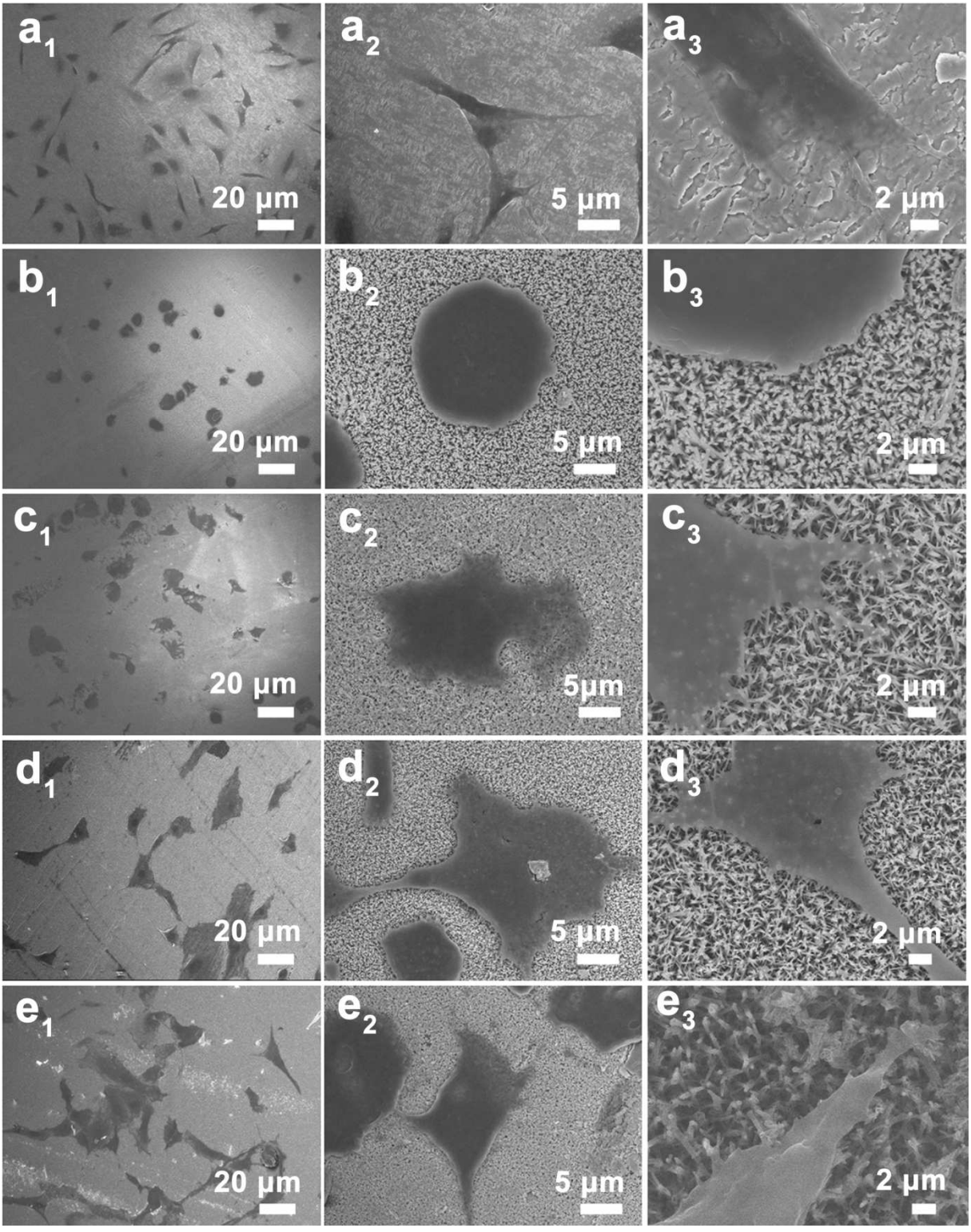

Fig. 10 SEM images of MC3T3-E1 cells cultured for 6 h on Ti (a_1-a_3), ZnO-NR (b_1-b_3), CS-NR (c_1-c_3), TA-NR (d_1-d_3), ZrO_2-NT (e_1-e_3).

cytocompatibility. On the other hand, ZrO_2-NT was proved to be a shelter with comparatively higher cell viability than Ti, CS-NR and TA-NR at any time, suggesting that the enhanced cell viability by ZrO_2-NT should be mainly related to smaller amount of Zn content.

3.6 Cytotoxicity

It is known that Zn is an essential trace element that has stimulatory effects on osteogenetic activity and bone formation at low concentration, while Zn overdose would lead to cytotoxicity.[15] Therefore, the level of LDH released from cells cultured on these samples was measured to assess the cytotoxicity. As shown in Fig. 12C, at each duration interval,

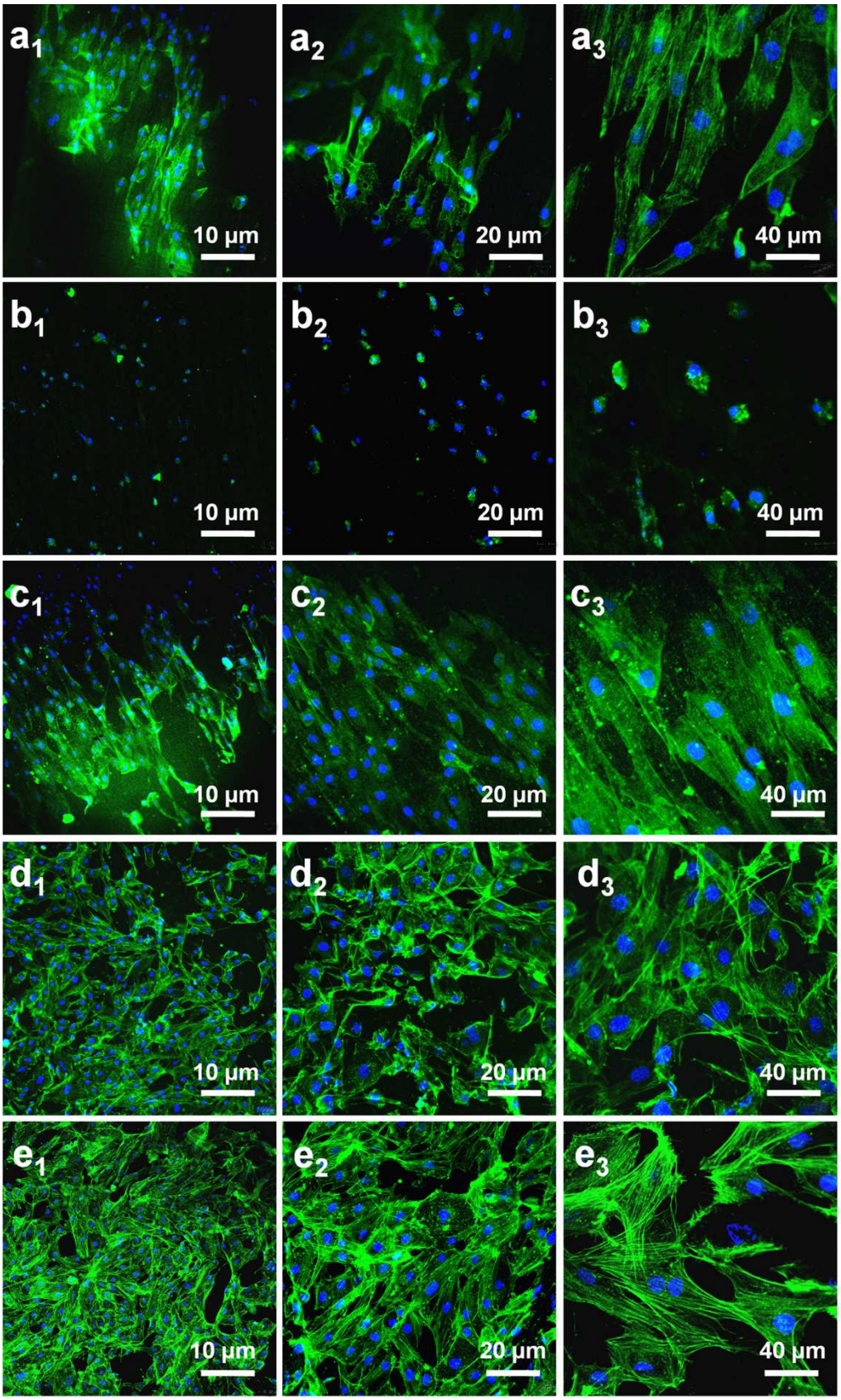

Fig. 11 Immunofluorescent images of cytoskeletal actin (green) and nuclei staining DAPI (blue) for MC3T3-E1 cells on Ti (a_1-a_3), ZnO-NR (b_1-b_3), CS-NR (c_1-c_3), TA-NR (d_1-d_3) and ZrO_2-NT (e_1-e_3) after 24 h of incubation.

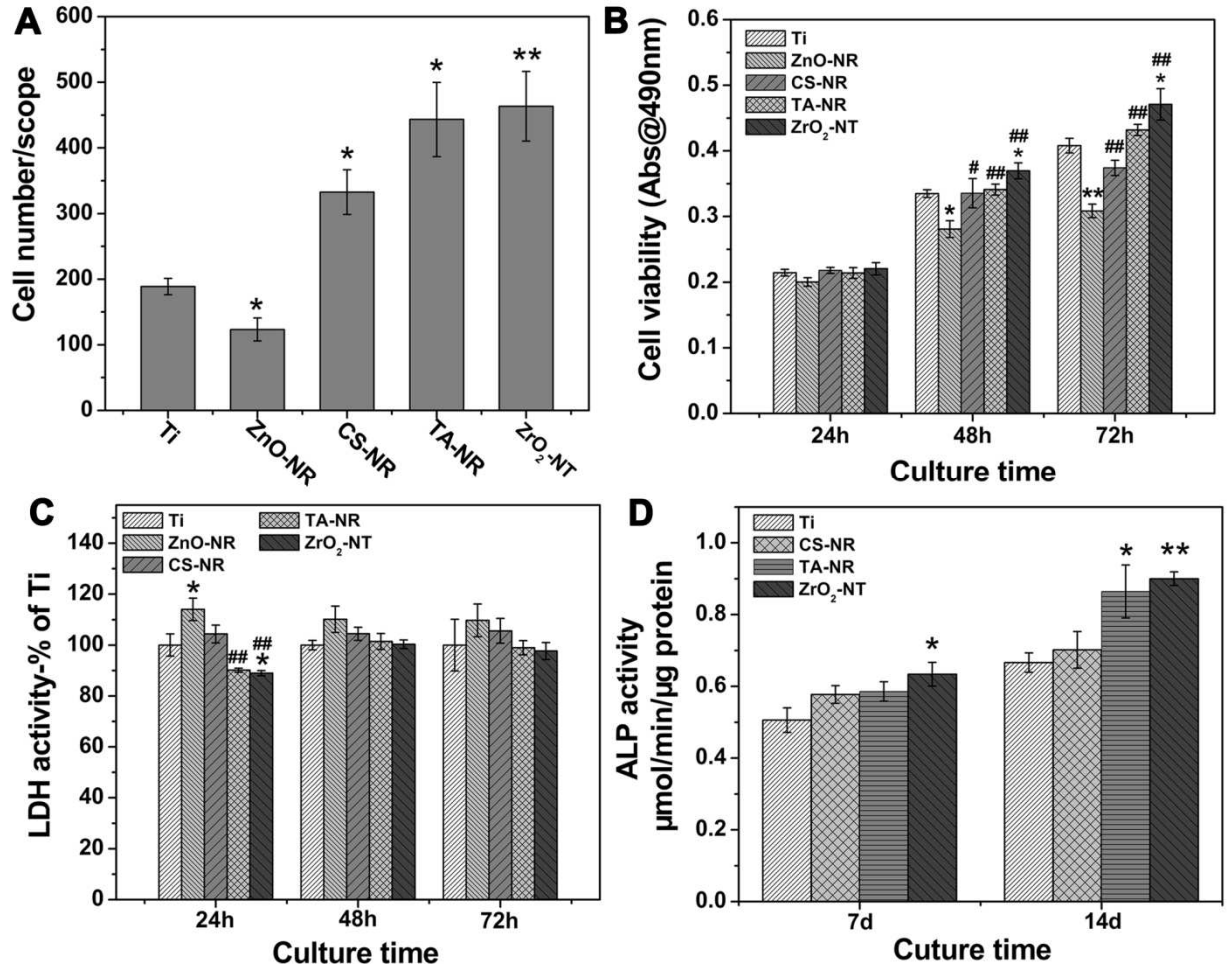

Fig. 12 (A) Adherent MC3T3-E1 number on different substrates after 24 h measured by counting cells displayed with DAPI; (B) MTT assay cell viability test showing the optical density (OD) of reaction product of the MTT working solution with MC3T3-E1 cells cultured on different substrates; (C) LDH activity in the culture media; (D) Alkaline phosphatase (ALP) activity of MC3T3-E1 cells after 7 and 14 d of incubation. Error bars represent mean ± SD for n = 5, *$p < 0.05$, **$p < 0.01$ compared to Ti and $^{\#}p < 0.05$ and $^{\#\#}p < 0.01$ compared to ZnO-NR.

ZnO-NR showed higher LDH activity than flat Ti, demonstrating strong cytotoxicity. LDH activity of CS-NR and TA-NR had no significant difference compared with flat Ti, whereas ZrO_2-NT exhibited much lower LDH activity than Ti did, illustrating no cytotoxicity or even better cytocompatibility.

3.7 ALP activity

In order to determine the early differentiation of MC3T3-E1 cells, ALP activity normalized according to total protein content was analyzed after the cells being cultured on different substrates for 7 and 14 days, respectively. As shown in Fig. 12D, the ALP activities on all samples showed a time dependent pattern. MC3T3-E1 cells cultured on CS-NR and TA-NR generated more ALP than those on Ti but the statistical difference was not obvious. For ZrO_2-NT, ALP was significantly up-regulated at either day 7 or 14 ($p< 0.05$ or $p< 0.01$), implying that the ZrO_2-NT had an advantage over others as a bioactive implant for it stimulated early bone formation better than others.

3.8 Osteogenesis-related gene expressions

To determine the osteogenic potential of MC3T3-E1 cells on different substrates, the gene expression of osteogenic markers, type Ⅰ collagen (Col-I), osteocalcin (OCN) and osteopontin (OPN) and bone morphogenetic protein 2 (BMP-2) were evaluated by real time-polymerase chain reaction (RT-PCR) after 14 days of culture.

The gene intensity of Col-I, one of the most important components of extracellular matrix in nature bone tissue,[33] was found to be reduced on all the Zn-incorporated nanoarrays when compared with that on Ti substrate after 14 days of incubation, although there was no significantly statistical difference between them (Fig. 13A). The mRNA level of OCN, a late marker for osteogenic differentiation,[34] was up-regulated on ZrO_2-NT when compared with pure Ti and other groups (Fig. 13B). Similar trend was also found in the mRNA level of OPN (Fig. 13C), one of the most abundant proteins in bone matrix. Remarkably, the gene expression of BMP-2, which plays a key role in skeletal development by inducing bone formation and regeneration, exhibited the highest level on the ZrO_2-NT substrate among all experimental groups (Fig. 13D).

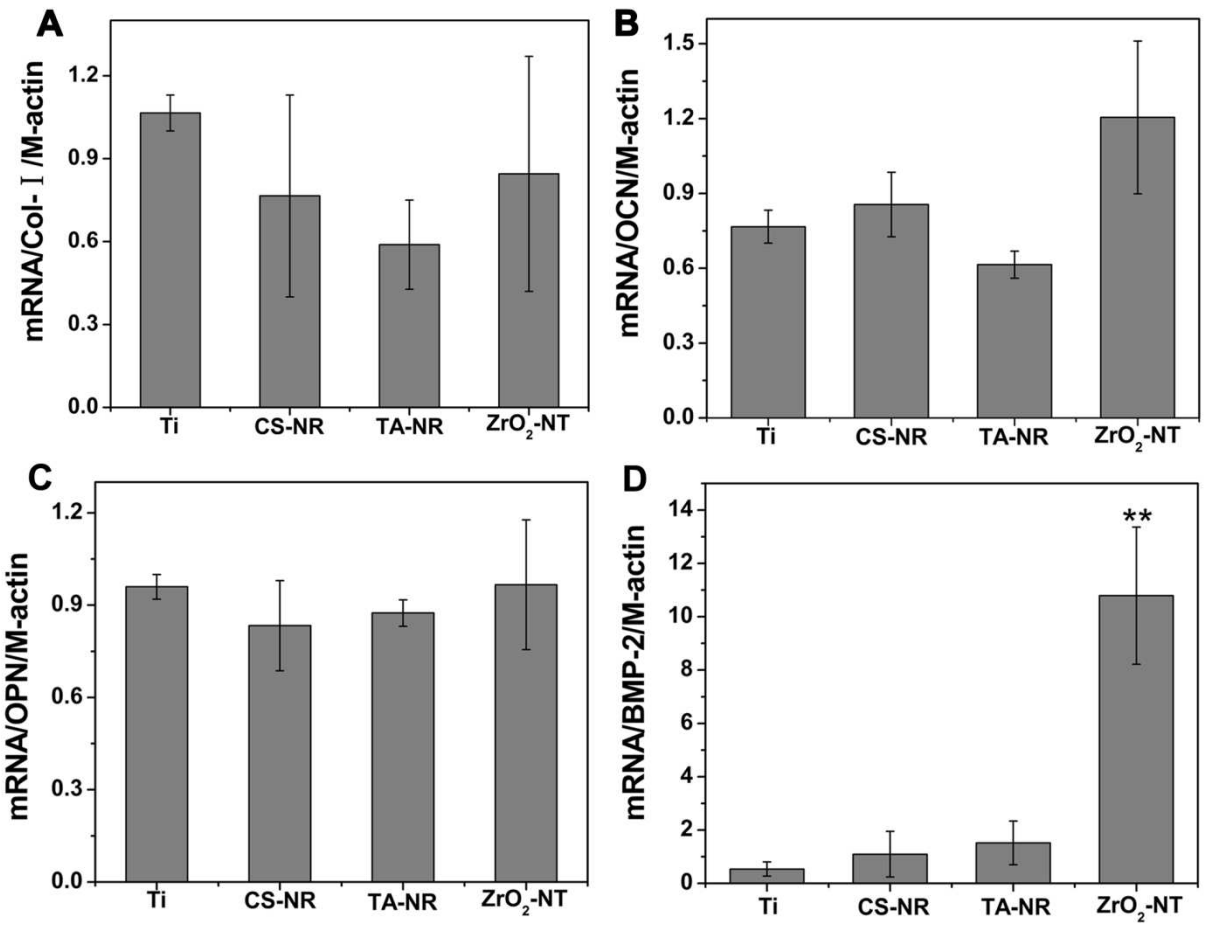

Fig. 13 Relative expressions of (A) Col-I, (B) OCN, (C) OPN and (D) BMP-2 by MC3T3-E1 cells cultured on different substrates for 2 weeks, all values normalized to M-actin. **p < 0.01 compared to Ti.

4. Discussion

Orthopaedic implant operation requires new materials with proper antibacterial property and sufficient osteogenetic activity to prevent millions of implant-associated infections worldwide. In order to obtain long-term antibacterial effect, the widely used approach in preparation of titanium-based antimicrobial drugs carrier system can be described as, the preparation of nanotubes by anodic oxidation method, followed by drug-loading into nanotubes by complex ways.[35-37] However, it still remains a challenge to deposit drugs uniformly into nanotubes and maintain its invariant morphology at the same time. On the other hand, excessive drugs accumulating out of nanotubes often leads to eruptible release and causes cell toxicity.[21]

In this study, we report novel bone implant materials with both favorable antibacterial control systems and high osteogenic activity and the results schematic can be seen in Fig. 14. Highly ordered ZnO nanorods with compatible density and dimensionality grown vertically on Ti substrate were employed as the morphology template. ZrO_2 was then integrated into the ZnO nanorods uniformly as a nanosized shell layer in the form of quasi-continuous nanoparticulates, with a large number of mesopore for Zn ion penetration and transportation, making it possible to provide long-term antibacterial effect. ZrO_2 coating not only precluded the direct contact between cell and ZnO nanorods, but also constructed suitable extracellular microenvironments for cell and enhanced biocompatibility of implants. The rough coating surface could strongly support osteoblasts adhesion and proliferation as reported by Wang et al.[38] As demonstrated in SEM image (Fig. 2d), there was more plenitudinous interconnecting space between the ZrO_2 nanotubes (~500nm) than common ZrO_2 nanotubes prepared by electrochemical anodization.[39] The high connectivity was more conducive for cell adhesion and proliferation for the reason that the structure make it easy for nutrient supply, gas diffusion, as well as metabolic waste removal, all of which contribute greatly f for the new bone formation.[40]

As it can be seen clearly in TEM images (Fig. 3), the content of ZnO could be easily controlled by condition of solution. The released Zn ion greatly influenced antibacterial property, biocompatibility and the expression of osteogenesis-related gene expression as depicted in Fig. 14. Actually, it can be inferred from this study that simutaneously good antibiosis and cytocompatibility is hardly achieved if Zn dosage was relatively high. Nevertheless a delicate balance between antibiosis and biocompatibility could be successfully reached by simply controlling the ZnO content and the Zn ions release.

The antibacterial effect was examined with both *S. aureus* and *E. coli*. It is well accepted that the great amount of active oxygen species produced by ZnO would disrupt the cell membranes.[41] Indeed, the SEM analysis (Fig. 7) confirmed that most of both bacteria species cultured with ZnO-NR, CS-NR, TA-NR and

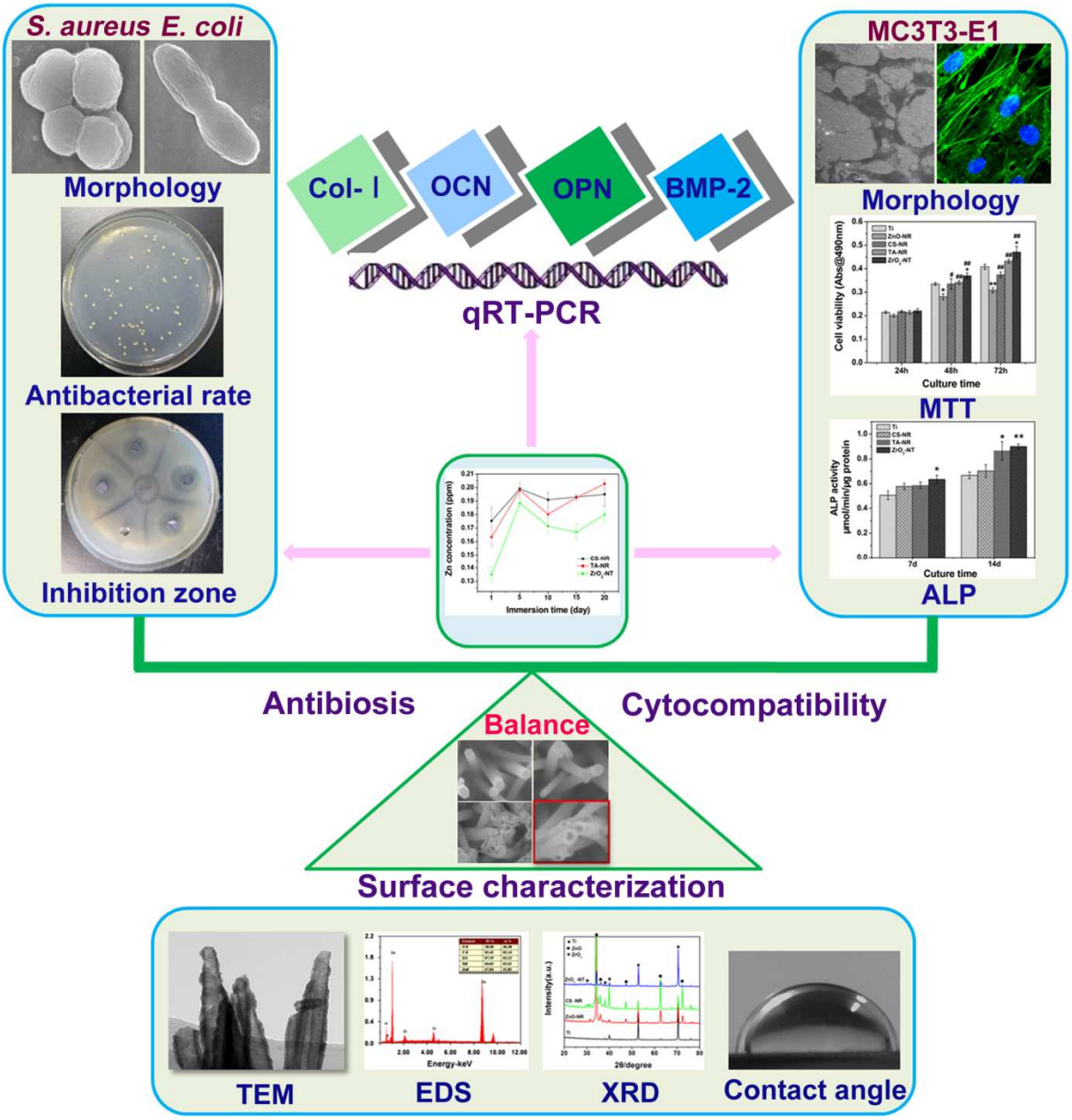

Fig. 14 Schematic illustration of the experiment results.

ZrO_2-NT were extensively injured on cell membranes. The integrity loss of the membranes further leads to malfunction of the permeability barrier, which ultimately caused the cell death.[42] It was reported that the release zinc ions could pierce the cell membranes and disturb bacteria functions by inhibition of the enzyme formation.[12] Typical pictures of recultivated *S. aureus* and *E. coli* colonies on agar plates manifest that all groups incorporated Zn show obvious inhibition on both bacteria.

As proved by previous research,[43] the reason for bacterial infections was the formation of biofilm on the surface of orthopedic implants. Reducing the number of viable bacteria is the most direct way to prevent biofilm formation. Making the interface of implant be rapidly covered with bistiocyte could prevent the implant from potential microbe adhesion effectively due to a living space competition.[44] MC3T3-E1 cells were cultured on different substrates to assess the cell-surface interactions. SEM (Fig. 10) images of adherent MC3T3-E1 cells on CS-NR, TA-NR and ZrO_2-NT revealed that cells spread well with noticeable filopodia extensions after incubation for the initial 6 hours. As one of the key signals for cell adhesion, filopodia is highly regulated by the reorganization of actin cytoskeleton and focal adhesion.[45] The analysis with fluorescence microscopy (Fig. 11) after 24 h demonstrated that MC3T3-E1 cells adhered to TA-NR and ZrO_2-NT substrates were typically polygonal, while they tended to be spindle on CS-NR and round on ZnO-NR. The cells density on ZnO-NR was much less than that on TA-NR and ZrO_2-NT. These results suggested ZnO nanorods were strong in antibacterial property, but they also exhibited toxicity to cells as they dissuaded the MC3T3-E1 cells adhesion and reduced the cell viability as well, which was

consistent with previous report that cells were unable to assemble focal adhesions and stress fibers on ZnO nanorods.[31]

For CS-NR, though ZnO was coated by ZrO_2 completely, the amount of ZnO incorporated was still more than that in TA-NR and ZrO_2-NT. Thus there were more Zn ions penetrating the ZrO_2 coating and accumulating in the culture medium, leading to slight cytotoxicity as demonstrated by the lower level of MTT formation and the higher level of released LDH compared to those of the Ti. It was suggested that the effect of Zn was dose dependent, as low dose Zn enhancing bone formation while ultrahigh doses inducing toxicity.[46] Previous research revealed that Zn ions at a concentration of 0.08-0.3ppm will have a positive effect on osteoblast functions and bone formation,[47,48] while in the range of 2-8 ppm, Zn ions can inhibits normal osteoblasts function via oxidative stress.[49]

In comparison with other substrates, ZrO_2-NT showed a significant increase in cell adhesion, activity and the lower LDH level. What's more, the early differentiation marker ALP activity detected in the ZrO_2-NT group was higher relative to other substrates. Due to the smallest amount of ZnO incorporated in the ZrO_2-NT, limited Zn ions were slowly released into the cell medium through the nanotubular structure, forestalling cytotoxicity-related problems observed in both ZnO-NR and CS-NR groups described above. It was found that the dosage as well as the possible biologic effect of Zn could be controlled by the content of ZnO and delivery of Zn ions.[50] Previous studies had revealed that the pharmacological performance of Zn-containing implants could be greatly influenced by the pattern of Zn release.[1] In general, slow and sustained release of Zn-incorporated implant material significantly enhanced osseointegration.[49] In this study, the ZrO_2-NT structure balances antibiosis and osteogenesis successfully, by inhibiting the growth of *S. aureus* and *E. coli* clearly and increasing the osseointegration *in vitro* by stimulating MC3T3-E1 cells adhesion and proliferation. It has been corroborated from several aspects that the unique nanotubular structure showed profound effects on the differentiation of MC3T3-E1 cells *in vitro*. The likely mechanism might be ascribed to regulation of ALP activity and expression of osteogenesis-related gene expression (Col-I, OCN, OPN and BMP-2). The novel drug-loaded nanotubular material was verified to improve the cellular activity on the surface, which is important for bone-implant contact *in vivo*.

5. Conclusion

In this study we reported direct evidence that an unique bifunctional effect for cellular activities and antibiosis, at least *in vitro*, could be obtained by means of carefully control the Zn content and release. The content of incorporated Zn can be easily controlled by pH value of HCl solution used in preparation of the nanostructures. All Zn-incorporated nanoarrays showed good antibacterial properties against both *E. coli* and *S.aureus*, as directly reflected by high antibacterial rates and apparent inhibition zone. Analysis of the biocompatibility confirmed that different hybrid nanoarrays could result in promotion for the adhesion and spreading of MC3T3-E1 cells to variable degrees. ZrO_2-NT could balance well the antibiosis and osteogenesis, at least *in vitro*, as proved by its good antibacterial effect as well as the up-regulated MTT and ALP activities, along with the increase of the osteogenesis-related gene expression of OCN, OPN and BMP-2 mRNA. The novel bone implant materials with better antibacterial property can promote the osteogenesis, which has promising and useful applications in biomedical devices and antibacterial control systems.

Acknowledgements

This work was supported by the the National Natural Science Foundation of China (No. 50802032 and 21103059), the Key Project of Natural Science Foundation of Hubei Province (No. 2011CDA092), the Key Scientific Project of Wuhan City (No. 2013011801010598), the Scientific Project of AQSIQ (No. 2013IK093) and self-determined research funds of CCNU from the colleges' basic research and operation of MOE (No.CCNU13A05007).

Notes and references

[a]*Institute of Nano-Science and Nano-Technology, College of Physical Science and Technology, Central China Normal University, Wuhan, 430079, China.. Fax: +86-2767861185; Tel: +86-2767861185; E- mail: zhzhu@phy.ccnu.edu.cn*

[b]*Hubei Key Laboratory of Genetic Regulation and Integrative Biology, School of Life Sciences, Central China Normal University, Wuhan, 430079, China. Fax: +86-2767861185; Tel: +86-2767861185; E- mail: ruili@mail.ccnu.edu.cn*

[c]*School of Life Sciences, Central China Normal University, Wuhan, 430079, China.*

[d]*College of Chemistry and Technology, Central China Normal University, Wuhan, 430079, China.*

‡*These authors contributed equally to this work.*

1. H. Hu, W. Zhang, Y. Qiao, X. Jiang, X. Liu and C. Ding, *Acta biomater.*, 2012, **8**, 904.
2. N. Høiby, T. Bjarnsholt, M. Givskov, S. Molin and O. Ciofu, *Int. J. Antimicrob. Agents*, 2010, **35**, 322.
3. O. Rzhepishevska, S. Hakobyan, R. Ruhal, J. Gautrot, D. Barbero and M. Ramstedt, *Biomater. Sci.,* 2013, **1**, 589.
4. K. Varaprasad, G. S. M. Reddy, J. Jayaramudu, R. Sadiku, K. Ramam and S. S. Ray, *Biomater. Sci.*, 2014, **2**, 257.
5. M. M. Fernandes, A. Francesko, J. Torrent-Burgués and T. Tzanov, *React. Funct. Polym.*, 2013, **73**, 1384.
6. D.-W. Lee, Y.-P. Yun, K. Park and S. E. Kim, *Bone*, 2012, **50**, 974.
7. A. Hoppe, V. Mouriño and A. R. Boccaccini, *Biomater. Sci.*, 2013, **1**, 254.
8. W. Jiang, H. Mashayekhi and B. Xing, *Environ. Pollut.*, 2009, **157**, 1619.
9. L. C. Ann, S. Mahmud, S. K. M. Bakhori, A. Sirelkhatim, D. Mohamad, H. Hasan, A. Seeni and R. A. Rahman, *Ceram. Int.*, 2014, **40**, 2993.
10. K. R. Raghupathi, R. T. Koodali and A. C. Manna, *Langmuir*, 2011, **27**, 4020.
11. A. Azam, A. S. Ahmed, M. Oves, M. S. Khan, S. S. Habib and A. Memic, *Int. J. Nanomed.*, 2012, **7**, 6003.
12. T. N. Phan, T. Buckner, J. Sheng, J. Baldeck and R. Marquis, *Oral microbiol. Immunol.,* 2004, **19**, 31.
13. F. Velard, D. Laurent-Maquin, J. Braux, C. Guillaume, S. Bouthors, E. Jallot, J.-M. Nedelec, A. Belaaouaj and P. Laquerriere, *Biomaterials*, 2010, **31**, 2001.
14. M. Roy, G. A. Fielding, A. Bandyopadhyay and S. Bose, *Biomater. Sci.*, 2013, **1**, 74.
15. K. Huo, X. Zhang, H. Wang, L. Zhao, X. Liu and P. K. Chu, *Biomaterials*, 2013, **34**, 3467.
16. I.-S. Kwun, Y.-E. Cho, R.-A. R. Lomeda, H.-I. Shin, J.-Y. Choi, Y.-H. Kang and J. H. Beattie, *Bone*, 2010, **46**, 732.
17. K. Yusa, O. Yamamoto, M. Fukuda, S. Koyota, Y. Koizumi and T. Sugiyama, *Biochem. Biophys. Res. Commun.*, 2011, **412**, 273.

18. N. Iitsuka, M. Hie and I. Tsukamoto, *Eur. J. Pharmacol.*, 2013, **714**, 41.
19. A. Gao, R. Hang, X. Huang, L. Zhao, X. Zhang, L. Wang, B. Tang, S. Ma and P. K. Chu, *Biomaterials*, 2014, **35**, 4223.
20. Q. Kang, Q. Z. Lu, S. H. Liu, L. X. Yang, L. F. Wen, S. L. Luo and Q. Y. Cai, *Biomaterials*, 2010, **31**, 3317.
21. M. S. Aw, M. Kurian and D. Losic, *Biomater. Sci.*, 2014, **2**, 10.
22. B. S. Necula, J. P. T. M. van Leeuwen, L. E. Fratila-Apachitei, S. A. J. Zaat, I. Apachitei and J. Duszczyk, *Acta biomater.*, 2012, **8**, 4191.
23. F. Y. Zhou, B. L. Wang, K. J. Qiu, L. Li, J. P. Lin, H. F. Li and Y. F. Zheng, *J. Biomed. Mater. Res. Part B*, 2013, **101B**, 237.
24. H.-L. Huang, Y.-Y. Chang, Y.-C. Chen, C.-H. Lai and M. Y. C. Chen, *Thin Solid Films*, 2013, **549**, 108.
25. Z. Lu, Z. Zhu, J. Liu, W. Hu and C. Ming Li, *Nanotechnology*, 2014, **25**, 215102.
26. S. Bauer, J. Park, J. Faltenbacher, S. Berger, K. von der Mark and P. Schmuki, *Integr. Biol.*, 2009, **1**, 525.
27. T. D. Zaveri, N. V. Dolgova, B. H. Chu, J. Lee, J. Wong, T. P. Lele, F. Ren and B. G. Keselowsky, *Biomaterials*, 2010, **31**, 2999.
28. J. Lellouche, A. Friedman, J. P. Lellouche, A. Gedanken and E. Banin, *Nanomed. Nanotechnol.*, 2012, **8**, 702.
29. Y. Wang, S. Zhang, X. Zeng, L. L. Ma, W. Weng, W. Yan and M. Qian, *Acta biomater.*, 2007, **3**, 191.
30. W.-q. Yu, X.-q. Jiang, F.-q. Zhang and L. Xu, *J. Biomed. Mater. Res. A*, 2010;**94A**:1012.
31. J. Lee, B. S. Kang, B. Hicks, T. F. Chancellor, Jr., B. H. Chu, H. T. Wang, B. G. Keselowsky, F. Ren and T. P. Lele, *Biomaterials*, 2008, **29**, 3743.
32. W. Song, J. Zhang, J. Guo, J. Zhang, F. Ding, L. Li and Z. Sun, *Toxicol. Lett.*, 2010, **199**, 389.
33. S. E. Bae, J. Choi, Y. K. Joung, K. Park and D. K. Han, *J. Control. Release*, 2012, **160**, 676.
34. Y. Hu, K. Cai, Z. Luo, Y. Zhang, L. Li, M. Lai, Y. Hou, Y. Huang, J. Li, X. Ding, B. Zhang and K. L. Paul Sung, *Biomaterials*, 2012, **33**, 3515.
35. K. C. Popat, M. Eltgroth, T. J. LaTempa, C. A. Grimes and T. A. Desai, *Biomaterials*, 2007, **28**, 4880.
36. H. Li, Q. Cui, B. Feng, J. Wang, X. Lu and J. Weng, *Appl. Surf. Sci.*, 2013, **284**, 179.
37. M.-Y. Lan, S.-L. Lee, H.-H. Huang, P.-F. Chen, C.-P. Liu and S.-W. Lee, *Ceram. Int.*, 2014, **40**, 4745.
38. G. Wang, X. Liu, H. Zreiqat and C. Ding, *Colloids Surf. B Biointerfaces*, 2011, **86**, 267.
39. C. J. Frandsen, K. S. Brammer, K. Noh, L. S. Connelly, S. Oh, L.-H. Chen and S. Jin, *Mater. Sci. Eng. C*, 2011, **31**, 1716.
40. H. Zreiqat, Y. Ramaswamy, C. Wu, A. Paschalidis, Z. Lu, B. James, O. Birke, M. McDonald, D. Little and C. R. Dunstan, *Biomaterials*, 2010, **31**, 3175.
41. S. Nair, A. Sasidharan, V. V. Divya Rani, D. Menon, S. Nair, K. Manzoor and S. Raina, *J. Mater. Sci. Mater. Med.*, 2009, **20**, 235.
42. G. Applerot, A. Lipovsky, R. Dror, N. Perkas, Y. Nitzan, R. Lubart and A. Gedanken, *Adv. Funct. Mater.,* 2009, **19**, 842.
43. J. T. Seil and T. J. Webster, *Acta biomater.*, 2011, **7**, 2579.
44. G. Subbiahdoss, B. Pidhatika, G. Coullerez, M. Charnley, R. Kuijer, H. C. van der Mei, M. Textor and H. J. Busscher, *Eur. Cell Mater.*, 2010, **19**, 205.
45. Y. Hu, K. Cai, Z. Luo, D. Xu, D. Xie, Y. Huang, W. Yang and P. Liu, *Acta biomater.*, 2012, **8**, 439.
46. E. Saino, S. Grandi, E. Quartarone, V. Maliardi, D. Galli, N. Bloise, L. Fassina, M. G. C. De Angelis, P. Mustarelli and M. Imbriani, *Eur. Cell Mater.* 2011, **21**, 59.
47. A. Hoppe, N. S. Güldal and A. R. Boccaccini, *Biomaterials*, 2011, **32**, 2757.
48. G. Jin, H. Cao, Y. Qiao, F. Meng, H. Zhu and X. Liu, *Colloids Surf. B Biointerfaces*, 2014, **117**, 158.
49. S. Miao, K. Cheng, W. Weng, P. Du, G. Shen, G. Han, W. Yan, S. Zhang, *Acta biomater.*,2008**, 4**, 441.
50. S. Miao, N. Lin, K. Cheng, D. Yang, X. Huang, G. Han, W. Weng and Z. Ye, *J. Am. Chem. Soc.,* 2011, **94**, 255.

Table of contents entry

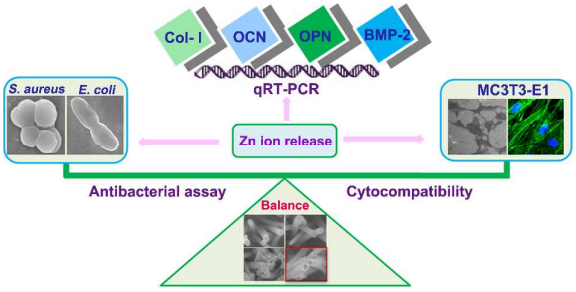

A bifunctional regulation in antibiosis and osteogenesis is obtained by well-organized Zn-incorporated ZrO_2 nanoarrays with interconnected internal space.